Enriched Free Mesh Method: An Accuracy Improvement for Node-based FEM

Genki Yagawa[1] and Hitoshi Matsubara[2]

[1] Center for Computational Mechanics Research, Toyo University, 2-36-5, Hakusan, Bunkyo-ku, Tokyo, Japan, 112-8611
yagawa@eng.toyo.ac.jp
[2] Center for Computational Science and Engineering, Japan Atomic Energy Agency, 6-9-3 Higashi-Ueno, Taito-ku, Tokyo, Japan, 110-0015
matsubara.hitoshi@jaea.go.jp

Summary. In the present paper, we discuss the accuracy improvement for the free mesh method: a node based finite element technique. We propose here a scheme where the strain field is defined over clustered local elements in addition to the standard finite element displacement field. In order to determine the unknown parameter, the least square method or the Hellinger-Reissner Principle is employed. Through some bench mark examples, the proposed technique has shown excellent performances.

1 Introduction

Recent advances in computer technology have enabled a number of complicated natural phenomena to be accurately simulated, which were ever only observed by experiments. Among various computer simulation techniques, the finite element method (hereinafter referred to as "FEM") has been most widely used due to the capability of analyzing an arbitrary domain, and results, accurate enough for engineering purposes, are obtainable at reasonable cost[1][2]. However, mesh generation for finite element analysis becomes very difficult and time consuming if the degree of freedom of the analysis model is extremely large, for example exceeding 100-million, and the geometries of the model are complex. In order to overcome the above shortcoming of the standard FEM, the so called mesh-free methods[3][4] have been studied. The Element-Free Galerkin Method (EFGM)[5][6] is among them with the use of integration by background-cells instead of by elements, based on the moving least square and diffuses element methods. The Reproducing Kernel Particle Method (RKPM)[7][8] is another mesh-free scheme, which is based on a particle method and wavelets. The general feature of these mesh-free methods is that, contrary to the standard FEM, the connectivity information between

Eugenio Oñate and Roger Owen (eds.), Computational Plasticity, 207–219.

nodes and elements is not required explicitly, since the evaluation of the total stiffness matrix is performed generally by the node-wise calculations instead of the element-wise calculations.

On the other hand, a virtually mesh-free approach called the free mesh method (hereinafter referred to as "FMM")[9][10] is based on the usual FEM, having a cluster of local meshes and equations constructed in a node-by-node manner. In other word, the FMM is a node-based FEM, which still keeps the well-known excellent features of the standard FEM. Through the node-wise manner of the FMM, a seamless flow in simulation procedures from local mesh generation to visualization of the results without user's consciousness is realized. The method has been applied to solid/fluid dynamics [11], crack problems[12], concrete problems[13], and so on. In addition, in order to achieve a high accuracy, the FMM with vertex rotations has been studied[14][15].

In this paper, we discuss another high accurate FMM: the Enriched FMM (hereinafter referred to as "EFMM"). In the following section, the fundamental concept of the original FMM is reviewed, and the third section deals with two EFMMs, one is "EFMM based on the localized least square method" and the other "EFMM based on the Hellinger-Reissner principle". In the fourth section, some numerical examples are presented, and concluding remarks are given in the final section.

2 Basic Concept of Free Mesh Method (FMM)

The FMM starts with only the nodes distributed in the analysis domain (Ω), without the global mesh data, as following equation.

$$p_i(x_i, y_i, r_i) \ \forall_i \in \{1, 2, \cdots, m\} \tag{1}$$

where m is the number of node, $p_i(x_i, y_i)$ are the Cartesian coordinates, and r_i is the nodal density information, which is used to generate appropriate nodes as illustrated in Fig. 1(a). From above nodal information, a node is selected as a central node and nodes within a certain distance from the central node are selected as candidate nodes. This distance is usually decided from the prescribed density of the distribution of nodes. Then, satellite nodes are selected from the candidate nodes, which generate the local elements around the central node (shown in Fig. 1(b)). For each local element, the element stiffness matrix is constructed in the same way as the FEM, however in FMM, only the row vector of stiffness matrix for each local element is necessary. The local stiffness matrix of each temporary element is given by

$$\mathbf{k}_{e_i} = [\, \mathbf{k}_{p_i} \ \mathbf{k}_{S_j} \ \mathbf{k}_{S_k} \,] \tag{2}$$

where $\mathbf{k}_{e_i}$ is the row vector of the stiffness matrix for element e_i and $\mathbf{k}_{p_i}$, $\mathbf{k}_{S_i}$ and $\mathbf{k}_{S_k}$ are components for node of p_i, S_i and S_k (j and k are number

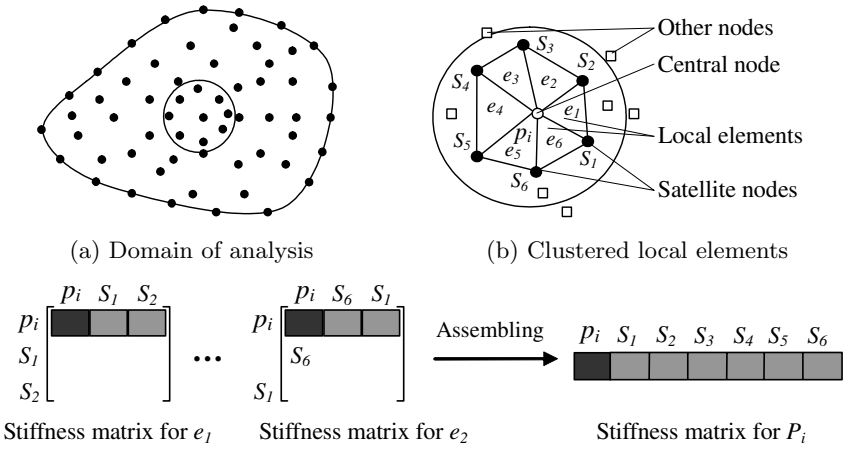

(a) Domain of analysis

(b) Clustered local elements

(c) Stiffness matrix for central node

Fig. 1. Concept of Free Mesh Method

of current satellite nodes). Through the above procedures are carried out for all local elements, the stiffness matrix for a central node is given by

$$\mathbf{k}_{p_i} = \sum_{i=1}^{n_e} \mathbf{k}_{e_i} \tag{3}$$

where $\mathbf{k}_{p_i}$ is the stiffness matrix for central node p_i, and n_e the number of local elements. Through the above procedures for all nodes is carried out, the global stiffness matrix is given by assembling $\mathbf{k}_{p_i}$ which are computed by node-wise manner:

$$\mathbf{K} = \begin{bmatrix} \mathbf{k}_{p_1} \\ \mathbf{k}_{p_2} \\ \vdots \\ \mathbf{k}_{p_m} \end{bmatrix} \tag{4}$$

Brief of the nodal stiffness matrix is shown in Fig. 1(c). After the construction of the global stiffness matrix, a derivation of the solution is processed. The great advantage of the FMM is that the global stiffness matrix can be evaluated in parallel with respect to each node through the node-wise manner, and only satellite node information is required with each nodal calculation. Finally, a derivation of the solution is performed as the usual FEM. Thus, the FMM is a node-wise FEM, which still keeps the well-known excellent features of the usual FEM. The features of FMM are summarized as follows,

(1) Easy to generate a large-scale mesh automatically
(2) Processed without being conscious of mesh generation
(3) The result being equivalent to that of the FEM

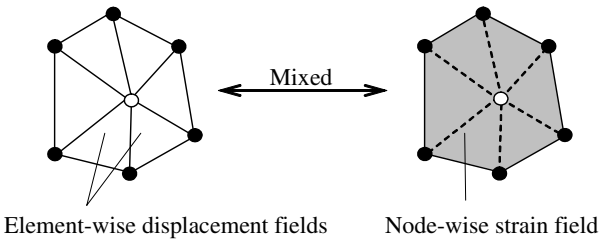

Fig. 2. Concept of enriched free mesh method

3 Enriched Free Mesh Method (EFMM)

3.1 Outline of EFMM

"Assumed strain on the clustered local elements" is the concept of EFMM as shown in Fig. 2. In the EFMM, the strain field on the clustered local elements and the displacement field of each local element are assumed independently. Relating these independent fields, we propose here two approaches, one is the localized least square method and the other is the method based on the Hellinger-Reissner principle.

3.2 EFMM Based on the Localized Least Square Method

The EFMM based on the localized least square method (hereinafter referred to as "EFMM-LS") assumes the strain field on the clustered local elements as

$$\{\varepsilon(\mathbf{x})\} = [\mathbf{N}^{\varepsilon}]\{\mathbf{a}\} \tag{5}$$

where $\{\varepsilon(\mathbf{x})\} = \{\varepsilon_{xx}, \varepsilon_{yy}, \gamma_{xy}\}$ is the strain field defined on the clustered local elements and each component of $\{\varepsilon_{xx}, \varepsilon_{yy}, \gamma_{xy}\}$ is assumed independently, and $[\mathbf{N}^{\varepsilon}]$ is a matrix, which consists of arbitrary polynomials as follows,

$$[\mathbf{N}^{\varepsilon}] = \begin{bmatrix} p^t(\mathbf{x}) & 0 & 0 \\ 0 & p^t(\mathbf{x}) & 0 \\ 0 & 0 & p^t(\mathbf{x}) \end{bmatrix} \tag{6}$$

where $p^t(x)$ is given on the clustered local elements as

$$\begin{array}{ll} p^t(\mathbf{x}) = \begin{bmatrix} 1 & x & y \end{bmatrix} & \textit{linear basis} \\ p^t(\mathbf{x}) = \begin{bmatrix} 1 & x & y & x^2 & xy & y^2 \end{bmatrix} & \textit{quadratic basis} \\ p^t(\mathbf{x}) = \begin{bmatrix} 1 & x & y & x^2 & xy & y^2 & x^3 & x^2y & xy^2 & y^3 \end{bmatrix} & \textit{cubic basis} \\ \cdots & \end{array} \tag{7}$$

In this paper, $p^t(x)$ is assumed to be linear or quadratic basis polynomial. The coefficients vector $\{\mathbf{a}\}$ in Eq. (5) is determined by minimizing the discrete L_2 norm as follows,

$$J = \sum_{c=1}^{n_e} \sum_{i=1}^{p} \left[\{\varepsilon(\mathbf{x})\} - \{\varepsilon_i^c\}\right]^2 \tag{8}$$

where n_e is the number of local elements with $c(= 1, 2, \cdots, n_e)$ being current local element, p the number of points, which are called as the "strain monitoring points" on the clustered local elements with $i(= 1, 2, \cdots, p)$ being the current strain monitoring point and $\{\varepsilon_i^c\}$the strain vector of i-th strain monitoring point on the c-th local element, which is called as the "mother element". The stationary condition of Eq. (8) is

$$\delta J = 2\{\mathbf{a}\}^T \sum_{c=1}^{n_e} \sum_{i=1}^{p} \left[[\mathbf{N}_i^\varepsilon]^T [\mathbf{N}_i^\varepsilon]\{\mathbf{a}\} - [\mathbf{N}_i^\varepsilon]^T \{\varepsilon_i^c\}\right] = 0 \tag{9}$$

which yields the coefficients vector $\{\mathbf{a}\}$ as follows,

$$\{\mathbf{a}\} = \sum_{c=1}^{n_e} \sum_{i=1}^{p} \left[\left[[\mathbf{N}_i^\varepsilon]^T [\mathbf{N}_i^\varepsilon] \right]^{-1} [\mathbf{N}_i^\varepsilon]^T \{\varepsilon_i^c\} \right] \tag{10}$$

Let us consider a simple Constant Strain Triangle as the mother element in which the displacement field of each local element is defined by

$$\{\mathbf{u}\} = \sum_{i=1}^{3} \{\mathbf{u}_i\} \zeta_i \tag{11}$$

where $\{\mathbf{u}\}$ is the displacement field of the local element, $\{\mathbf{u}_i\}$ is the nodal displacement, and ζ_i is the area-coordinate[16]. Thus, the strain value on the strain monitoring points is given by

$$\{\varepsilon_i^c\} = [\mathbf{B}_i^c]\{\mathbf{u}_i\} \tag{12}$$

where

$$\begin{aligned} &[\mathbf{B}_i^c] = \left[[\mathbf{B}_1] \; [\mathbf{B}_2] \; [\mathbf{B}_3] \right] \\ &with \\ &[\mathbf{B}_j] = \begin{bmatrix} \partial\zeta_j/\partial x & 0 \\ 0 & \partial\zeta_j/\partial y \\ \partial\zeta_j/\partial y & \partial\zeta_j/\partial x \end{bmatrix} \quad , \quad j = 1, 2, 3 \end{aligned} \tag{13}$$

By substituting Eq. (12) into Eq. (10), the unknown coefficient $\{\mathbf{a}\}$ is determined as

$$\{\mathbf{a}\} = \sum_{c=1}^{n_e} \sum_{i=1}^{p} \left[\left[[\mathbf{N}_i^\varepsilon]^T [\mathbf{N}_i^\varepsilon] \right]^{-1} [\mathbf{N}_i^\varepsilon]^T [\mathbf{B}_i^c] \{\mathbf{u}_i\} \right] \tag{14}$$

Substituting Eq. (14) into Eq. (15), we obtain

$$\{\varepsilon(\mathbf{x})\} = [\mathbf{N}^{\varepsilon}] \sum_{e=1}^{n_e} \sum_{i=1}^{p} \left[[[\mathbf{N}_i^{\varepsilon}]^T [\mathbf{N}_i^{\varepsilon}]]^{-1} [\mathbf{N}_i^{\varepsilon}]^T [\mathbf{B}_i^{c}] \{\mathbf{u}_i\} \right] = [\mathbf{A}] \{\mathbf{u}_i\} \tag{15}$$

where

$$[\mathbf{A}] = [\mathbf{N}^{\varepsilon}] \sum_{e=1}^{n_e} \sum_{i=1}^{p} \left[[[\mathbf{N}_i^{\varepsilon}]^T [\mathbf{N}_i^{\varepsilon}]]^{-1} [\mathbf{N}_i^{\varepsilon}]^T [\mathbf{B}_i^{c}] \right] \tag{16}$$

In the elasticity problem, the stress vector $\{\sigma\}$ and the strain vector $\{\varepsilon\}$ have the relation as follows,

$$\{\sigma\} = [\mathbf{D}] \{\varepsilon\} \tag{17}$$

where $[\mathbf{D}]$ is a symmetric matrix of material stiffness. With $[\mathbf{D}]$ given by Eq. (16), the stiffness matrix based on the localized least square method is computed on the clustered local elements as

$$[\mathbf{k}_{LS}] = \int_{\Omega} [\mathbf{A}]^T [\mathbf{D}] [\mathbf{A}] \mathbf{d}\Omega \tag{18}$$

where Ω is area of the clustered local elements. It is important to say that the above stiffness matrix is computed in a node-wise manner.

It is noted that the present EFMM-LS is closely related to the superconvergent patch recovery proposed by Zienkiewicz and Zhu[17][18]. In an adaptive finite element method[19][20], the Z-Z error estimator has been most widely used to estimate the error. The error estimator requires an exact solution, but generally it is impossible to compute the exact value because the exact solution is not available in general. The Z-Z technique then obtains the recovered solution in a post processing stage. The clustered local elements in the present method are equivalent to the superconvergent patch used in the Z-Z technique. The difference lies in that the recovering procedure in the EFMM-LS is in a main process stage when computing element stiffness matrices. The use of the assumed strain is therefore, in some sense, equivalent to the "post-process" of the Z-Z superconvergent patch recovery.

3.3 EFMM Based on Hellinger-Reissner Principle

In the EFMM based on the Hellinger-Reissner principle [1][21] (hereinafter referred to as "EFMM-HR"), the Hellinger-Reissner (hereinafter referred to as "HR") principle is employed to obtain better accuracy. Let the HR principle of a linear elastic body be defined on the clustered local elements by

$$\begin{aligned} \prod(\varepsilon, \mathbf{u}) = \int_{\Omega} \{\varepsilon\}^{\mathbf{T}} [\mathbf{D}] \{\partial \mathbf{u}\} d\Omega - \frac{1}{2} \int_{\Omega} \{\varepsilon\}^{\mathbf{T}} [\mathbf{D}] \{\varepsilon\} d\Omega \\ - \int_{\Omega} \{\mathbf{u}\}^{\mathbf{T}} \{\mathbf{b}\} d\Omega - \int_{S_{\sigma}} \{\mathbf{u}\}^{\mathbf{T}} \{\tilde{\mathbf{t}}\} dS \end{aligned} \tag{19}$$

where

$$\{\partial \mathbf{u}\} = [\mathbf{B}]\{\bar{\mathbf{u}}\} \ , \ \{\varepsilon\} = [\mathbf{N}^{\varepsilon}]\{\bar{\varepsilon}\} \tag{20}$$

with $\{\mathbf{b}\}$ being the applied body force per unit mass, and $\{\tilde{t}\}$ the applied traction on boundary S_σ. $\{\bar{\mathbf{u}}\}$ is the unknown nodal displacement and $\{\bar{\varepsilon}\}$ the unknown nodal strain. The unknown values $(\bar{\mathbf{u}}, \bar{\varepsilon})$ of the HR principle satisfy the following equations in a weak manner,

$$\int_{\Omega} \delta\{\varepsilon\}^{\mathbf{T}}[\mathbf{D}]\left([\mathbf{B}]\{\bar{\mathbf{u}}\} - [\mathbf{N}]\{\bar{\varepsilon}\}\right) d\Omega = 0 \tag{21}$$

$$\int_{\Omega} \delta\{\mathbf{u}\}^{\mathbf{T}}[\mathbf{B}]^{\mathbf{T}}[\mathbf{D}][\mathbf{N}]\{\bar{\mathbf{u}}\}d\Omega - \int_{\Omega} \delta\{\mathbf{u}\}^{\mathbf{T}}\{\mathbf{b}\}d\Omega - \int_{S_\sigma} \delta\{\mathbf{u}\}^{\mathbf{T}}\{\tilde{\mathbf{t}}\}dS = 0 \tag{22}$$

It is noted here that the strain field is defined on the clustered local elements by node-wise manner, where the displacement field is defined on each element by element-wise manner. Equations (21) and (22) yields the following linear matrix equation,

$$\begin{bmatrix} -\mathbf{A} & \mathbf{C} \\ \mathbf{C}^{\mathbf{T}} & \mathbf{0} \end{bmatrix} \begin{Bmatrix} \bar{\varepsilon} \\ \bar{\mathbf{u}} \end{Bmatrix} = \begin{Bmatrix} \mathbf{f_1} \\ \mathbf{f_2} \end{Bmatrix} \tag{23}$$

where

$$\begin{cases} \mathbf{A} = \int_{\Omega} [\mathbf{N}^{\varepsilon}]^{\mathbf{T}}[\mathbf{D}][\mathbf{N}^{\varepsilon}]d\Omega \\ \mathbf{C} = \int_{\Omega} [\mathbf{N}^{\varepsilon}]^{\mathbf{T}}[\mathbf{D}][\mathbf{B}]d\Omega \\ \mathbf{f_1} = 0 \\ \mathbf{f}_2 = \int_{\Omega} [\mathbf{N}^{u}]^{\mathbf{T}}\{\mathbf{b}\}d\Omega + \int_{\Gamma} [\mathbf{N}^{u}]^{\mathbf{T}}\{\tilde{t}\}d\Gamma \end{cases} \tag{24}$$

By condensing the coefficient matrix of Eq. (23), we obtain the following equation,

$$\mathbf{C}^T\left(\mathbf{A}^{-1}\mathbf{C}\bar{\mathbf{u}}\right) = \mathbf{f_2} \tag{25}$$

where the condensation should be executed on the clustered local elements. Thus, the stiffness matrix based on the HR principle is computed on the clustered local elements as follows,

$$[\mathbf{k}_{HR}] = \mathbf{C}^T\mathbf{A}^{-1}\mathbf{C} \tag{26}$$

It is noted here that we can obtain the enriched stiffness matrix without increasing the number of nodal degrees of freedom.

4 Examples

4.1 Convergence Study: Displacement

To study the convergence characters of the present methods, a cantilever model is solved as shown Fig. 3, where the three different mesh patterns are prepared and the mesh division in the x direction is varied. As shown in the figure, a beam of length $L = 10$, height $D = 1$ and thickness $t = 1$

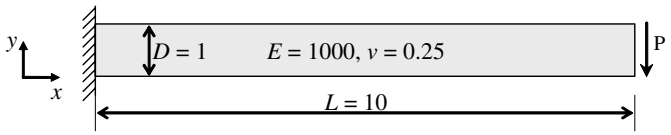

(a) Cantilever beam model

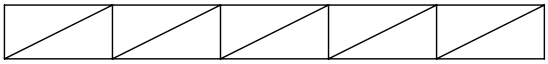

(b) One layer mesh

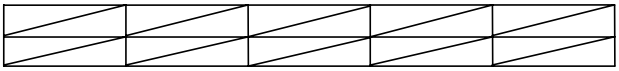

(c) Two layers mesh

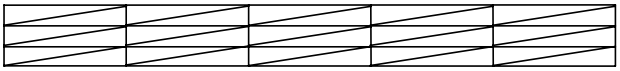

(d) Three layers mesh

Fig. 3. Mesh patterns for cantilever beam model

is subjected to a shear load in plane stress condition. The material parameters are given as the Young's modulus $E = 1000.0$ and the Poisson's ratio $\nu = 0.25$. The displacements at the loaded edge normalized by the exact value are plotted against the degrees of freedom (see Fig. 4). From the comparison of displacement results among the six different solutions, it can be observed that

(a) The accuracy of the FEM with the three noded linear element of constant strain is the worst, whereas that with the six noded quadratic element is the best irrespective of the mesh patterns.
(b) As the number of layers in the thickness direction increase, the accuracy of EFMMs approaches that of the quadratic FEM.
(c) Regarding the comparisons among the EFMMs, the accuracy of the EFMM-HR and the EFMM-LS with the linear strain field are the best, whereas, for the finer meshes (see Fig. 4(c)), the results of EFMMs with the quadratic strain field are almost equivalent to those of the formers.

4.2 Convergence Study: Error Norms

As another convergence measures, two kinds of error norms for the beam problems as shown Fig. 5 [22] are employed, which are, respectively, given as

$$\|E\|_2 = \left[\int_\Omega \left(\mathbf{u} - \mathbf{u}^{exact}\right)^T \left(\mathbf{u} - \mathbf{u}^{exact}\right) d\Omega\right]^{1/2} \tag{27}$$

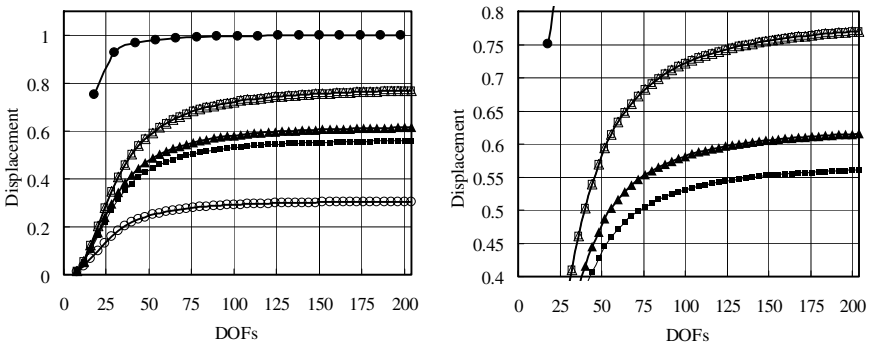

(a) One layer mesh

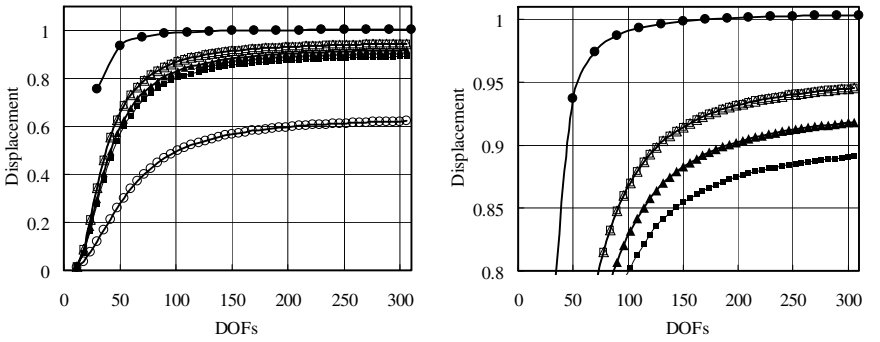

(b) Two layer mesh

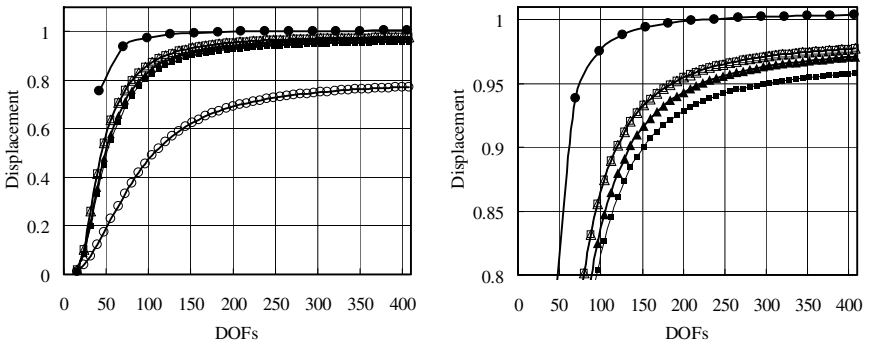

(c) Three layer mesh

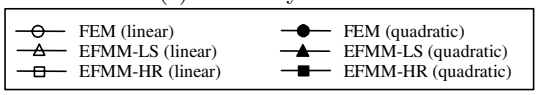

Fig. 4. Normalized displacements at the loaded edge vs. DOFs (The figures in the right hand side are zoomed ones)

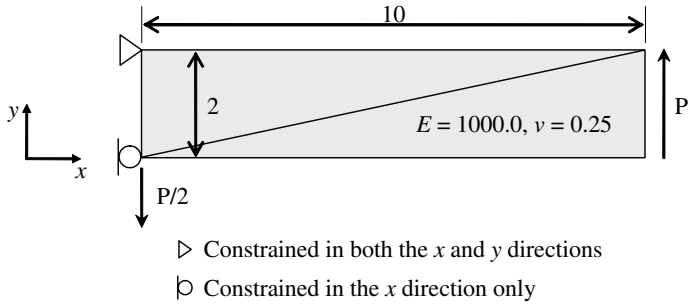

Fig. 5. Cantilever beam model for error norm study; only the case of mesh is shown as examples

$$\|E\|_e = \left[\int_\Omega \frac{1}{2}\left(\varepsilon - \varepsilon^{exact}\right)^T \left(\sigma - \sigma^{exact}\right) d\Omega\right]^{1/2} \tag{28}$$

where $\|E\|_2$ is the displacement error norm and $\|E\|_e$ that of the energy error. $\mathbf{u}$, ε and σ are, respectively, the numerical results of displacement, strain and stress, whereas $\mathbf{u}^{exact}$, $\varepsilon^{\mathbf{exact}}$ and $\sigma^{\mathbf{exact}}$ are the exact solutions. A beam of length $L = 10$, height $D = 2$ and thickness $t = 1$ is subjected to a shear load in plane stress condition. The material parameters are given by the Young's modulus $E = 1000.0$ and the Poisson's ratio $\nu = 0.25$. The above displacement and energy convergence norms are plotted against the DOFs in Figs. 6 and 7, respectively, where the meshes are, respectively, 1×1, 2×2, 4×4, 16×16, 32×32, and 64×64. It can be seen from these figures that

(a) Again, the error norms of the displacement of the EFMMs are between those of the linear and the quadratic FEMs (see Fig. 6). However, the convergence slopes of the EFMMs are almost equal to that of the quadratic FEM.
(b) The error norms of the energy of the quadratic EFMMs are almost the same as that of the quadratic FEM and those of the linear EFMMs are between the linear and the quadratic FEMs.

4.3 Patch Test

The patch test is performed using the three models of patch as shown in Fig. 8, where the displacement field

$$\begin{Bmatrix} u(x) \\ v(y) \end{Bmatrix} = \begin{Bmatrix} 0.2x \\ -0.6y \end{Bmatrix} \tag{29}$$

is applied at the boundary. Table 1 shows the test results for the FEMs and the EFMMs. As illustrated in the table, all the method passes the patch test for the Model A, which is a regular mesh division model. However, for the Model B and C, which are irregular ones, the EFMM-LSs do not pass the

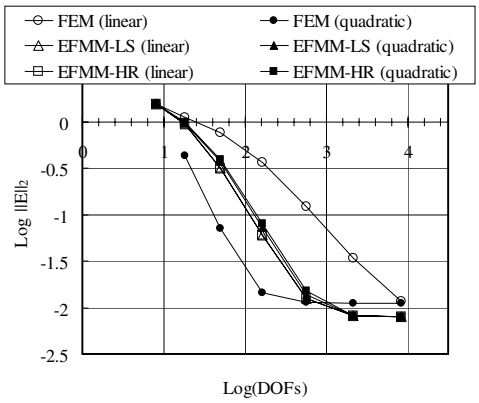

Fig. 6. L_2 error norms of displacement vs. DOFs

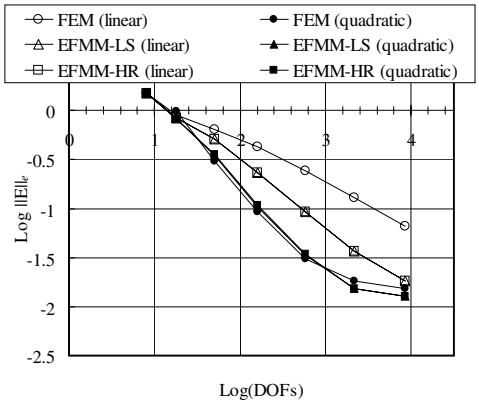

Fig. 7. Energy error norms vs. DOFs

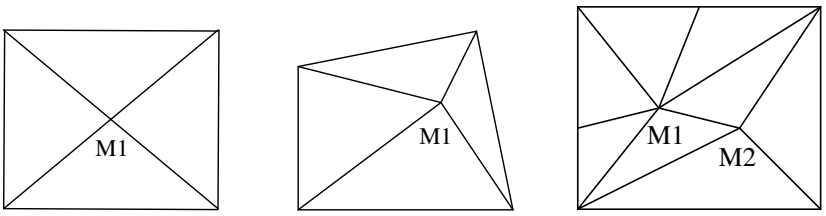

(a) Model A (b) Model B (c) Model C

Fig. 8. Models for patch tests

test. Here, "Pass" means that the displacement of the internal node ($M1$ or $M2$) satisfies Eq. (29). This means that the EFMM-LSs are nonconforming for irregular mesh, which is an open question.

Table 1. Displacements at internal nodes $M1$ and $M2$

	Model A		Model B		Model C			
	$u(M1)$	$v(M1)$	$u(M1)$	$v(M1)$	$u(M1)$	$v(M1)$	$u(M2)$	$v(M2)$
FEM(linear)	0.900	-2.400	1.200	-3.000	0.600	-2.400	1.300	-1.800
FEM(quadratic)	0.900	-2.400	1.200	-3.000	0.600	-2.400	1.300	-1.800
EFMM-LS(linear)	0.900	-2.400	1.198	-3.170	0.611	-2.372	1.285	-1.899
EFMM-LS(quadratic)	0.900	-2.400	1.198	-3.141	0.611	-2.368	1.290	-1.859
EFMM-HR(linear)	0.900	-2.400	1.200	-3.000	0.600	-2.400	1.300	-1.800
EFMM-HR(quadratic)	0.900	-2.400	1.200	-3.000	0.600	-2.400	1.300	-1.800
Exact	0.900	-2.400	1.200	-3.000	0.600	-2.400	1.300	-1.800

5 Concluding remarks

A new Free Mesh Method called "Enriched Free Mesh Method" is proposed in this paper, in which a high accuracy can be obtained without explicitly increasing the degree of freedoms. The work is summarized as follows,

(1) The key idea of the proposed method is that the strain field is assumed on clustered local elements, in addition to the usual displacement field on each element. To relate the above two fields, the localized least square method or the Hellinger-Reissner principle are, respectively, employed.
(2) The convergence characteristics of the displacement L2 error norms in the cantilever problem are between that of the FEM with the linear displacement field and that with the quadratic one, whereas that of the energy error norms with the quadratic strain field for the clustered elements is equivalent to that of the FEM with the quadratic displacement field.
(3) The EFMM based on the Hellinger-Reissner principle passes the patch test, whereas, for irregular nodal arrangements, the EFMM based on the localized least square method does not. This would be an open question and there is a room for future research.

References

1. Zienkiewicz OC, Taylor RL (2000) The finite element method. Fifth edition, Butterworth Heinemann
2. Cook RD, Malkus DS, Plesha ME (1989) Concepts and applications of finite element analysis. Third edition, Wiley
3. Barth TJ, Griebel M, Keyes DE, Nieminen RM, Roose D, Schlick T (2003) Meshfree methods for partial differential equation. Springer-Verlag Berlin Heidelberg
4. Liu GR, Liu MB (2003) Smoothed Particle Hydrodynamics a meshfree particle method. World Scientific publishing
5. Belytschko T, Lu YY, Gu L (1994) Element-free Galerkin methods. Int J Num Meth Engng 37:229–256
6. Lu YY, Belytschko T, Gu L (1994) A new implementation of the element-free Galerkin Method. Comput Meth Appl Mech Engng 113:397–414

7. Liu WK, Jun S, Adee J, Belytischko T (1995) Reproducing kernel particle methods for structural dynamics. Int J Num Meth Engng 38:1655–1680
8. Liu WK, Li S, Belytschko T (1997) Moving least square kernel particle method Part 1: methodology and convergence. Comput Meth Appl Mech Engng 143:113–154
9. Yagawa G, Yamada T (1996) Free mesh method: a new meshless finite element method. Computational Mechanics 18:383–386
10. Yagawa G, Furukawa T (2000) Recent developments approaches for accurate free mesh method. Int J Num Meth Engng 47:1445–1462
11. Fujisawa T, Inaba M, Yagawa G (2003) Parallel computing of high-speed compressible flows using a node-based finite-element method. Int J Num Meth Engng 58:481–511
12. J. Imasato, Y. Sakai (2002) Application of 2-dimentional crack propagation problem using FMM. Advances in Meshfree and X-FEM Methods, Liu GR, editor, World-Scientific
13. Matsubara H, Iraha S, Tomiyama J, Yagawa G (2002) Application of 3D free mesh method to fracture analysis of concrete. Advances in Meshfree and X-FEM Methods, Liu GR, editor, World-Scientific
14. Matsubara H, Iraha S, Tomiyama J, Yamashiro T, Yagawa G (2004) Free mesh method using a tetrahedral element including vertex rotations. JSCE J of Structural Mechanics and Earthquake Engineering 766(I-68):97–107
15. Tian R, Matsubara H, Yagawa G, Iraha S, Tomiyama J (2004) Accuracy improvement on free mesh method: a high performance quadratic tetrahedral/triangular element with only corners. Proc of the 2004 Sixth World Congress on Computational Mechanics (WCCM VI)
16. O.C. Zienkiewicz, K. Morgan (1983), Finite element and approximation, John Wiley & Sons
17. Zienkiewicz OC, Zhu JZ (1992) The superconvergent patch recovery and a posteriori error estimates. PART 1: The recovery technique. Int J Num Meth Engng 33:1331–1364
18. Zienkiewicz OC, Zhu JZ (1992) The superconvergent patch recovery and a posteriori error estimates. PART 2: Error estimates and adaptivity. Int J Num Meth Engng 33:1365–1382
19. Zienkiewicz OC, Zhu JZ (1992) The superconvergent patch recovery (SPR) and adaptive finite element refinement. Comput Meth Appl Mech Engng 101:207–224
20. Babuska I, Rheinboldt WC (1978) A-posteriori error estimates for the finite element method. Int J Num Meth Engng 12:1597–1615
21. Washizu K (1968) Variational methods in elasticity and plasticity. Pergamon Press, New York
22. Timoshenko SP, Goodier JN (1987) Theory of elasticity. McGraw-Hill